# GMI Instrument Spin Balance Method, Optimization, Calibration and Test

Laoucet Ayari*, Michael Kubitschek*, Gunnar Ashton*, Steve Johnston*, Dave Debevec*,
David Newell* and Joseph Pellicciotti**

## Abstract

The Global Microwave Imager (GMI) instrument must spin at a constant rate of 32 rpm continuously for the 3-year mission life. Therefore, GMI must be very precisely balanced about the spin axis and center of gravity (CG) to maintain stable scan pointing and to minimize disturbances imparted to the spacecraft and attitude control on-orbit. The GMI instrument is part of the core Global Precipitation Measurement (GPM) spacecraft and is used to make calibrated radiometric measurements at multiple microwave frequencies and polarizations. The GPM mission is an international effort managed by the National Aeronautics and Space Administration (NASA) to improve climate, weather, and hydro-meteorological predictions through more accurate and frequent precipitation measurements. Ball Aerospace and Technologies Corporation (BATC) was selected by NASA Goddard Space Flight Center to design, build, and test the GMI instrument. The GMI design has to meet a challenging set of spin balance requirements and had to be brought into simultaneous static and dynamic spin balance after the entire instrument was already assembled and before environmental tests began. The focus of this contribution is on the analytical and test activities undertaken to meet the challenging spin balance requirements of the GMI instrument. The novel process of measuring the residual static and dynamic imbalances with a very high level of accuracy and precision is presented together with the prediction of the optimal balance masses and their locations.

## Introduction

The GMI instrument is one of the payload instruments on the GPM core spacecraft and must be spun continuously at 32 revolutions per minute (rpm) ± 0.1% on-orbit for the 3-year operational life of the instrument and to provide the desired geo-location for the science data. Details pertaining to the GMI design and testing were presented in references [1, 2]. The GMI instrument had to be spun balanced to less than 0.032 kg-m (2.77 lbm-in) static imbalance and less than 0.055 kg-m$^2$ (188 lb-in$^2$) dynamic imbalance, total imbalance, for the 123-kg spinning portion of the instrument payload. The design and development of the spin balance method, analytical solution, test setup, design, calibration, and measured test results are described. The verification and validation of the GMI instrument to demonstrate compliance of performance through environmental testing and spin balance has been successfully completed. At the writing of this contribution, GMI has been fully integrated onto the GPM spacecraft, and the GPM spacecraft has been shipped to the launch site in Tanegashima, Japan for launch in February 2014.

The static and dynamic balancing approach consists of spinning GMI on top of an accurately calibrated dynamometer, designed specifically for GMI to measure the imparted forces due to imbalance. This device continues a long tradition of building precision balancing machines, vibration input benches and force measurement instruments for space hardware at Ball Aerospace & Technologies Corporation [5,6].

The dynamometer measures all forces and moments and consists of three force transducers mounted to an aluminum base plate and a corresponding top plate that functions as the mounting interface for the GMI instrument (Figure 1). The calibration of the dynamometer showed that the total measurement error of this technique and dynamometer were much smaller, by an order of magnitude, than the imbalance

---

* Ball Aerospace & Technologies Corporation, Boulder, CO

** NASA Goddard Space Flight Center, Greenbelt, MD

requirements. Since the balance requirements were tight and the spin balance to be measured was so small, the structural resonances of the GMI instrument, as well as the spin balance test fixture and support structure, also required detailed modeling and design to meet stiffness requirements dictated by the imbalance accuracies to be measured. Figure 2 shows the finite element model of the GMI instrument, the model of the Thermal Vacuum (TVAC) support structure with the dynamometer assembly used for the spin balance, and locations of balance masses available on the GMI instrument.



**Figure 1.  Dynamometer Assembly Setup in Calibration and GMI without RDA and MR Assemblies Integrated**
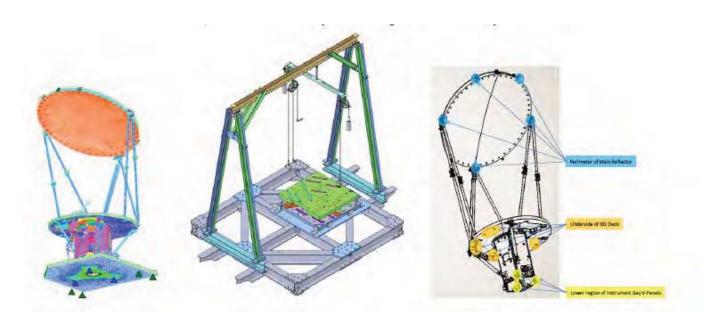


**Figure 2.  (a) Structural Model of the GMI Instrument Assembly, (b) Dynamometer**

**with the Spin Balance Test Fixture, and (c) Balance mass locations on GMI**

Multiple test setups, shown in part in Figures 2 and 3, were developed for balancing GMI at room temperature and in a vacuum chamber to eliminate error terms associated with forces imparted to the dynamometer due to air drag of the GMI instrument spinning in air. A MATLAB computer program was developed to process the resultant forces imparted on the dynamometer, together with position encoder data to derive the magnitude and direction of static and dynamic imbalances, and subsequently perform a linear optimization to predict the optimal balance mass solution. This optimal solution, which meets the static and dynamic imbalance requirements, consists of the values of 21 'balance' masses that can be added and accounts for design constraints specific to each of the balance mass locations, and at the same time minimizing the overall total mass of balance masses to be added simultaneously. The optimization can account for order of preference in the choice of masses by assigning higher weights for particular ones to reflect certain particularities such as ease of access, volume or other situational constraints or preferences. Finally, it has been possible to achieve preliminary balancing of GMI before achieving full integration. The software is capable of balancing a partially integrated GMI while the instrument is being assembled (e.g., before the integration of the RDA – Reflector Deployment Assembly and MR – Main Reflector) by assigning negative inertial properties to the missing subassemblies that were subcontracted elsewhere and would not be integrated for the spin balance testing until late in the environmental test program.

## Spin Balance Verification

The GMI instrument underwent an initial spin balance in the clean room in July 2011 and initial balance masses were added prior to GMI instrument environmental testing. Final spin balance and requirement verification and validation was completed in TVAC in February 2012 after the GMI instrument had successfully completed all environmental testing (Figure 3). The methods and steps successfully accomplishing this spin balance of the GMI instrument and showing the requirement was verified via test measurements will be discussed in this paper.



**Figure 3.  GMI Instrument in Spin Balance Test Facility on Dynamometer**

Evaluation of Imbalance Forces

Bringing GMI into balance started from early on in the design phase. As the design progressed, there has been a continuous effort to keep the rotating hardware as close as possible to static and dynamic balance in order to minimize overall total mass of the instrument, with a plan for three separate axial and radial locations to place balancing masses as shown in Figure 2-c. While a minimum of two axial planes for balance masses are required to achieve dynamic balancing, provision to use the RDA/MR for a third location was necessary to maintain lower added masses, because the RDA does not have axial symmetry, is distant from the mounting plane, and due to other production and schedule constraints.

The basic idea is to determine the static and dynamic imbalances from the measurements of the moving imbalance forces imparted at the mounting plane while spinning GMI at some angular velocity. Load cells are ideal for the task as they only pick variations in load magnitudes. In the absence of other disturbances, such as structural resonances, air drag, etc., it can be easily shown that the loads imparted by a non-perfect rotating device on a mounting plane are the result of the centrifugal forces and moments of the imperfection. Assuming an imbalance mass $m$ centered at a position $(x,y,z)$ in the GMI reference frame of Figure 4, the reactions are given by the following radial force $\boldsymbol{f_r}$ and the radial moment $\boldsymbol{M_r}$
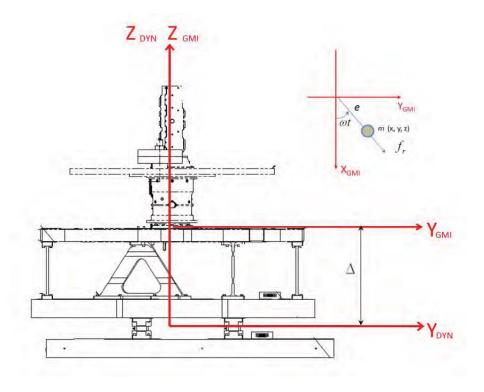


**Figure 4. GMI and Dynamometer Coordinate systems**

$$\boldsymbol{f_r} = \begin{Bmatrix} f_x \\ f_y \end{Bmatrix} = me\omega^2 \begin{Bmatrix} \cos \omega t \\ \sin \omega t \end{Bmatrix} = m\omega^2 \begin{Bmatrix} x \\ y \end{Bmatrix}, \tag{1}$$

$$\boldsymbol{M_r} = \begin{Bmatrix} M_{rx} \\ M_{ry} \end{Bmatrix} = z \begin{Bmatrix} -f_x \\ +f_y \end{Bmatrix} + mg \begin{Bmatrix} -y \\ +x \end{Bmatrix} = \omega^2 \begin{Bmatrix} -m\,yz \\ +m\,xz \end{Bmatrix} + mg \begin{Bmatrix} -y \\ +x \end{Bmatrix} = \omega^2 \begin{Bmatrix} -i_{yz} \\ +i_{xz} \end{Bmatrix} + \frac{g}{\omega^2} \begin{Bmatrix} -f_x \\ +f_y \end{Bmatrix}, \tag{2a}$$

where $e = \sqrt{x^2 + y^2}$ is the radial distance from the spin axis, $\omega$ is the angular velocity, $g$ is the magnitude of gravitational acceleration and $t$ is the time in seconds. Note that we replaced the products $m\,yz$ and $m$

*xz* by the cross products of inertia $i_{yz}$ and $i_{xz}$, respectively in the last equality of Equation (2a) to account for pure dynamic imbalance situations and therefore address the general case of arbitrary combined static and dynamic imbalances. All forces and moments are functions of time. For example, $M_r$ should be written as $M_r(t),$ but the time symbol is omitted for readability. From the dynamometer we can read the exact forces, but the moments will be different due to the height $\Delta$, between the mount interface and the elevation of the load cells. On the dynamometer, the readings for the moments are given by:

$$\begin{Bmatrix} M_x \\ M_y \end{Bmatrix} = \begin{Bmatrix} M_{rx} \\ M_{ry} \end{Bmatrix} + \Delta \begin{Bmatrix} -f_y \\ +f_x \end{Bmatrix} = \omega^2 \begin{Bmatrix} -i_{yz} \\ +i_{xz} \end{Bmatrix} + \left( \frac{g}{\omega^2} + \Delta \right) \begin{Bmatrix} -f_y \\ +f_x \end{Bmatrix} \tag{2b}$$

The resultant force in the Z direction is independent of time and therefore would not show on the dynamometer readings since the load cells measure only a change in force. The radial load remains unchanged but the lever arm of the moment is increased by the distance between the mounting surface and the plane of the dynamometer load cells.

Using the expression for the radial load from Equation (1), the magnitude of the radial load is related to the static imbalance *me* via

$$me = m\sqrt{x^2 + y^2} = \sqrt{f_x^2 + f_y^2} = \frac{\|f_r\|}{\omega^2} \tag{3}$$

In order to address the dynamic imbalance requirement, we use Equation (3). The dynamic imbalance is related to the imbalance forces and moments as following:

$$J_{rz} = \left\| \begin{Bmatrix} -i_{yz} \\ +i_{xz} \end{Bmatrix} \right\| = \frac{1}{\omega^2} \left\| M_r - \left( \frac{g}{\omega^2} + \Delta \right) \begin{Bmatrix} -f_y \\ +f_x \end{Bmatrix} \right\| \quad \text{or} \tag{4}$$

$$J_{rz} = \left\| i_{rz}^{\perp} \right\| = \frac{1}{\omega^2} \left\| M_r - \left( \frac{g}{\omega^2} + \Delta \right) f_r^{\perp} \right\| \text{ where } f_r^{\perp} = \begin{Bmatrix} -f_y \\ +f_x \end{Bmatrix} \text{ and } i_{rz}^{\perp} = \begin{Bmatrix} -i_{yz} \\ +i_{xz} \end{Bmatrix}.$$

The requirements for static and dynamic balancing have to be compared to the values obtained from the product *me* and $J_{rz}$ computed from Equations (3) and (4) respectively. In addition to the magnitudes of the static and dynamic imbalances, of practical interest are their corresponding directions. To find the precise directions, two coordinate systems can be set on the test setup. One is stationary relative to the dynamometer, while the second rotates with the GMI unit. These two coordinate systems share an origin and the z-axis and initially both x-axes and y-axes are co-linear. Since the angle at which GMI has rotated is known, we can subtract that from the direction of the resultant force to find the physical direction of the imbalance via

$$\theta_f = \tan^{-1} \left( \frac{f_y}{f_x} \right) - \theta_{GMI} \tag{5}$$

$$\theta_M = \tan^{-1} \left( \frac{M_y - \Delta \cdot f_x}{M_x + \Delta \cdot f_y} \right) - \theta_{GMI} \tag{6}$$

We have just established that the static and dynamic imbalances form a pair of vectors that may be plotted in a three-dimensional graph to graphically pinpoint the directions of the imbalances together with the physical locations of the balance masses to visually help the technical team understand which masses will be most effective.

Optimal Balancing Using Linear Programming
Having determined the levels of static and dynamic imbalances, we now determine the optimal balance masses that would simultaneously make the radial force and moment on the dynamometer nil. In order for GMI to be statically balanced, its center of mass must reside on the axis of rotation. This can be done

by creating equal and opposite forces to the resultant x and y forces imbalance forces, expressed through the following equality constraints

$$\sum_{i=1}^{n} m_i x_i = -\frac{f_r}{\omega^2} \cos \theta_f \ , \tag{7}$$

$$\sum_{i=1}^{n} m_i y_i = -\frac{f_r}{\omega^2} \sin \theta_f \ . \tag{8}$$

where $m_i$ is the $ith$ balancing mass of coordinates $x_i, y_i \ and \ z_i, \ i = 1..n.$, and $\theta_f$ is the angle of the imbalance radial force. Similarly, the moments created by the dynamic imbalance must be counteracted by the added balancing masses making the combined cross product of inertia nil resulting in the following additional two constraint equations

$$\sum_{i=1}^{n} m_i x_i \left( z_i + \frac{g}{\omega^2} \right) = -\frac{M_r}{\omega^2} \sin \theta_M \tag{9}$$

$$\sum_{i=1}^{n} m_i y_i \left( z_i + \frac{g}{\omega^2} \right) = \frac{M_r}{\omega^2} \cos \theta_M \tag{10}$$

Because the locations of the balancing masses are known, we have a system of four linear equilibrium Equations (7-10) to $n$ unknown mass values $m_i$ , $i = 1 \ldots n$. For the case of GMI, we have $n$ = 21. There is no unique solution to this over-determined problem. However, an optimal unique solution may be found by writing a linear programming problem in which we minimize the sum of the balance masses while meeting the static and dynamic balance equality constraints (7-10) and introducing inequality constraints on the balance masses that take into account the feasibility of actual mass placement with respect to size/mass constraints of the balance mass for a given location and the positive nature of the balance masses. The objective function to be minimized is expressed as

$$\varphi(\boldsymbol{m}) = \sum_{i=1}^{n} \alpha_i m_i = \boldsymbol{\alpha}^T \boldsymbol{m} \tag{11}$$

And the optimization problem is written formally as

$$\min_{m}(\boldsymbol{\alpha}^T \boldsymbol{m}) \text{ such that } \begin{cases} \mathbf{A}eq \cdot \mathbf{m} = \mathbf{b}eq \\ \boldsymbol{lb} < \boldsymbol{m} < \boldsymbol{ub} \end{cases} \tag{12}$$

The matrix equation $\mathbf{A}eq \cdot \mathbf{m} = \mathbf{b}eq$ is the set of four equality constraints described above and is set up as shown in Equation (13).

$$\begin{bmatrix} x_1 & x_2 & \dots & x_n \\ y_1 & y_2 & \dots & y_n \\ x_1\left(z_1 + \frac{g}{\omega^2}\right) & x_2\left(z_2 + \frac{g}{\omega^2}\right) & \dots & x_n\left(z_n + \frac{g}{\omega^2}\right) \\ y_1\left(z_1 + \frac{g}{\omega^2}\right) & y_2\left(z_2 + \frac{g}{\omega^2}\right) & \dots & y_n\left(z_n + \frac{g}{\omega^2}\right) \end{bmatrix} \begin{bmatrix} m_1 \\ m_2 \\ \vdots \\ \vdots \\ \vdots \\ m_n \end{bmatrix} = \begin{bmatrix} -\frac{f_r}{\omega^2} \cos \theta_f \\ -\frac{f_r}{\omega^2} \sin \theta_f \\ -\frac{M_r}{\omega^2} \sin \theta_M \\ \frac{M_r}{\omega^2} \cos \theta_M \end{bmatrix} \tag{13}$$

The expression $\boldsymbol{lb} < \boldsymbol{m} < \boldsymbol{ub}$ represents a set of 2n inequality constraints that set the lower and upper bounds on the balance masses. The lower bound must be set to zero, as we are adding mass, and the

upper bound must be a set of mass values that can be handled given the physical reality of space available at each balance mass location. They could also turn off certain masses that are difficult to access due to some practical envelope constraints. The linear problem given by Equation (12) is solvable using MATLAB's linear programming function "linprog" using the same software that collects dynamometer sensor data and encoder position as the test unit spins atop of the dynamometer.

## Calibration of the Dynamometer Setup

The calibration entails three parts. In the first part, the dynamometer is shown to have the necessary sensitivity to accurately make the necessary measurements needed to process the imbalance data. The noise floor of the dynamometer is identified and compared to the requirements on forces and moments that are derived to meet GMI's static and dynamic balancing requirements.

In the second part of the calibration, the forces measured by the dynamometer are checked using two separate data acquisition systems and two loading methods. This was performed to isolate and quantify the sources and magnitudes of systematic and random measurement errors. Finally, the third part in the calibration program evaluates data collected from auxiliary risk mitigation tests which used the GMI SMA (Spin Mechanism Assembly) and simulated payloads with off-axis known masses precisely located on a rotating disk (see Figure 4). These mitigation tests were planned to assess the performance of the tools to be used in the actual balancing of GMI. Three test cases were performed. The first one has a moderate imbalance, while the second test case is intended to achieve extreme static and dynamic imbalances. Finally, the third test case is intended to produce a balanced state from which we demonstrate the capability of the system to meet the required level of balance measurements for GMI.

Specified and Derived Requirements
The two GMI balancing requirements are expressed in terms of the product $me \leq 0.032$ kg-m (2.77 lb-in) for static imbalance and $J_{rz} \leq 0.055$ kg-m$^2$ (187 lb-in$^2$) for dynamic imbalance. We derive two equivalent requirements that provide the equivalent limits on the static and dynamic imparted forces and moments that GMI needs to meet in order for the balancing effort to be successful. These requirements are shown to be for the radial force $\leq 0.08$ lb (0.36 N) and the radial moment $\leq 10$ in-lb (1.1 N-m). In addition, a requirement on the noise floor is set so that accurate and reliable measurements of the balanced state are performed. The noise floor of the dynamometer is checked against 1/10$^{th}$ of the requirement levels, padded by a 50% uncertainty levied to account for unknown error contributions to the measurements. The noise floor is found to be $\leq 0.004$ lb (0.018 N) for reliable measurements to occur.

Using the expression for the radial load from Equation (1) and using an angular frequency of 0.533 Hz (32 rpm), the magnitude of the radial load is related to the imbalance $me$ via

$$me = \frac{\|f_r\|}{\omega^2} \quad \Rightarrow \quad \|f_r\| = me\omega^2 = 0.032 \ (2\pi \ 0.533)^2 = 0.36N \ (0.08 \ \text{lb})$$

Furthermore, de-rating this level by 50% to account for unknowns in the setup, we need to bring the radial load to less than 0.04 lb (0.18 N) if we want to show that GMI is statically balanced. Thus, we need to have a noise floor level less than 0.004 lb (0.018 N). In order to address the dynamic balance requirement, we use Equation (3). We have the magnitude of the radial moment given by:

$$\|M_r\| = \left\| \omega^2 \begin{Bmatrix} -i_{yz} \\ +i_{xz} \end{Bmatrix} + \left( \frac{g}{\omega^2} + \Delta \right) \begin{Bmatrix} -f_y \\ +f_x \end{Bmatrix} \right\| \leq \left\| \omega^2 \begin{Bmatrix} -i_{yz} \\ +i_{xz} \end{Bmatrix} \right\| + \left\| \left( \frac{g}{\omega^2} + \Delta \right) \begin{Bmatrix} -f_y \\ +f_x \end{Bmatrix} \right\| = \omega^2 J_{rz} + \left( \frac{g}{\omega^2} + \Delta \right) \|f_r\|$$

$$\|M_r\| \leq J_{rz}\omega^2 + me\left( g + \Delta\omega^2 \right) = 0.055(2\pi \times 0.533)^2 + 0.032(9.81 + 16.455 \times 0.0254(2\pi \times 0.533)^2)$$

$$\|M_r\| \leq 1.08 \ Nm \quad (< 10 \ \text{in-lb})$$

Again, de-rating this level by 50% to account for unknowns in the setup, we need to bring the radial moment to less than 0.6 N-m (5 in-lb) if we want to show that GMI is statically balanced. Thus, we need to have a noise level less than 1/10th of 0.056 N-m (0.496 in-lb). Considering the forces in the sensors from which we compute the moments and the geometry shown in Figure 5, the noise floor needs to be less than 0.5 in-lb (0.06 N-m) /(26.035/2.54) or 0.05 lb (0.22 N). Accounting for three sensors, we have to have a noise floor better than 0.016 lb (0.071 N). In summary, the requirement imposed on the noise floor of the radial force is 0.004 lb (0.018 N) and the one imposed on the moments is 0.5 in-lb (0.06 N-m) (that is 0.016 lb (0.071 N) in force sensors). The smaller value of the two is 0.004 lb (0.018 N) and is kept for comparison with the performance of the dynamometer.
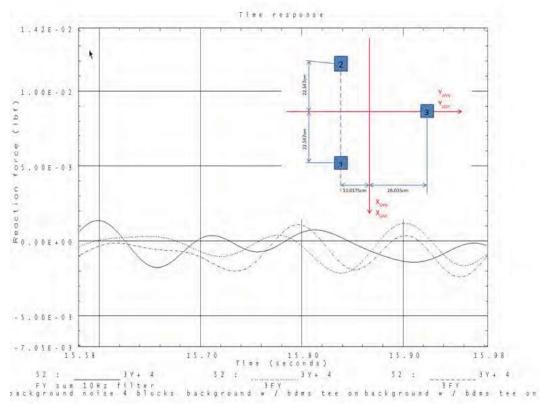


**Figure 5. Noise floor showing measurements filtered using low bandpass of 10 Hz**

To measure the noise floor, the dynamometer was placed on four blocks at the four corners of the lower plate. This configuration was chosen instead of the fully clamped one to simulate the actual balancing configuration in which the dynamometer's own mode is in the vicinity of 30 Hz versus the 120 Hz+ in the fully clamped configuration. Three measurements were taken. In the first measurement, the data from the load cells is channeled only to an independent secondary data acquisition system (VXI system). In the second test, the data from the load cells is channeled to the BDMS data acquisition (processor to be used for balancing) and simultaneously to the VXI through a set of "T" connections. The third test has both data acquisition systems in place except that the data acquisition card of the BDMS was turned off. A digital filter of 10 Hz was applied to the data sets. An example of dynamometer noise floor measurement for the Y-axis is shown in Figure 5. The maximum noise of 0.00175 lb (0.00778 N) is measured and is found to be less than the 0.004 lb (0.018 N) needed to carry out accurate measurements to meet GMI spin balance requirements.

Harmonic stinger test
This test is intended to calibrate the measurements performed by the dynamometer as a system. The dynamometer is excited at a frequency of 10 Hz using an MTB 50-lb (220-N) stinger. A calibrated load cell is placed at the interface between the stinger and the dynamometer to measure the input force. The

latter was also measured using the dynamometer as the sum of the contributions of all load cells. The load is applied along the Y direction of the dynamometer. The input loads matched the output load. The Spectral Dynamics Data Acquisition System of BATC's Vibration Lab was also used to further check the response and the results. They were found to be identical to the reference load.

Frequency response function (FRF) tests

The FRF shows that the data is unaffected by the fundamental modes of the dynamometer either in a clamped or a simply supported configuration. The difference in loads is negligible in the vicinity of 0.5 Hz. While the results of the excitation illustrated in Figures 6 and 7 are for the Y-axis, similar results are recovered for the X-axis. The FRF was also measured prior to balancing GMI either in the clean room or in the vacuum chamber BRUTUS where additional modes are present due to the mounting equipment. The mount and fixture hosting GMI during spin balance testing in the BRUTUS vacuum chamber is analyzed using the finite element method incorporating a GMI model to ensure that we have no interference from the added structural resonance modes. The mounting beams in BRUTUS (Figure 2b) were stiff enough and produce no modes that interfere with measurements.

Speaker tests

The goal of the dynamic calibration using a speaker load input is to verify that we are reading the correct dynamic loads while balancing the GMI instrument, no matter where these loads are applied over the dynamometer. The calibration consists in applying known forces using a speaker precisely oriented and located at different elevations over the dynamometer and measure the reaction forces and moments imparted on the surface of the dynamometer. The speaker is attached to a fixture through an encapsulated load cell to ensure a precise knowledge of the magnitude and location of the excitation. The speaker is actuated using a form generator to deliver an accurate input frequency. The test shows the input load from the speaker force transducer and the measurement from the dynamometer are the same in different orientations. In particular, this test is required to verify the correctness of the measured moments which are crucial for dynamic imbalance predictions.

Risk Mitigation Balance Tests

In order for the GMI balancing task to run smoothly, a risk reduction set of tests were carried using the SMA drive and a flywheel on which known masses are placed in well-known locations on the flywheel as shown in Figure 8. The first test consists of the placement of an imbalance mass of about 1.1-lb (4.9-N) at the edge of the flywheel. The second test is an extreme case created by a 16-lb (71-N) imbalance, also placed at the edge of the flywheel. Finally, the last case is of a situation in which an attempt was made to balance the flywheel and the SMA to the best available capabilities. The results of this test points to how a balanced situation results in very small shear and moment loads exported to the mount of the SMA. The data from the dynamometer is compared to the mass tally data. It is found that accurate estimates of the imbalance can be made using the dynamometer. In addition, a balanced state can be easily identified once the shear force and moment become small.

In the first test case, a set of known imbalance masses were placed on the bare flywheel. Knowing the location of the masses, a static imbalance of 13.491 in-lb (1.5243 N-m) and a dynamic imbalance of 139.077 lb-in$^2$ (0.040699 kg-m$^2$) are computed. The total mass of the added hardware consisting of studs, washers and spacers weighs 1.1075 lb (4.9264 N) and its center of mass is located at a radius of 12.18 in (30.93 cm). The radial force and radial moment maintain a nearly constant value as the SMA and its payload rotate. The mean static and dynamic imbalances given by Equations (4) and (5) are computed over a period of 70 seconds at a rate of 1 KHz. These values are within 1% of the expected values as shown in Table 1. The second test is an extreme case in which 18.20 lb (80.95 N) is placed at the edge of the flywheel to produce an imbalance which is about 100 times the imbalance requirement. The static and dynamic imbalances are about 270 lb-in (30.5 N-m) and 2900 lb-in$^2$ (0.8487 kg-m$^2$) respectively. The total mass of the added hardware consisted of two dumbbells, studs, washers and spacers is 18.2025 lb (80.9688 N). Again, the radial force and radial moment maintained constant values as the SMA and its flywheel payload with imbalance mass rotate and the system recovered the static and dynamic imbalances with errors of 0.41% and 1.8% respectively. In the third test case, the measured mean

resultant radial load of 0.015 lb (0.067 N) is below the requirement of 0.08 lb (0.36 N), and the measured mean resultant moment of 0.51 in-lb (0.06 N-m) is below the 10 in-lb (1.1 N-m) equivalent requirement. This last test provided the necessary argument that the system is capable of predicting a balanced state.

**Table 1. Comparison of measured imbalance to correction magnitudes**

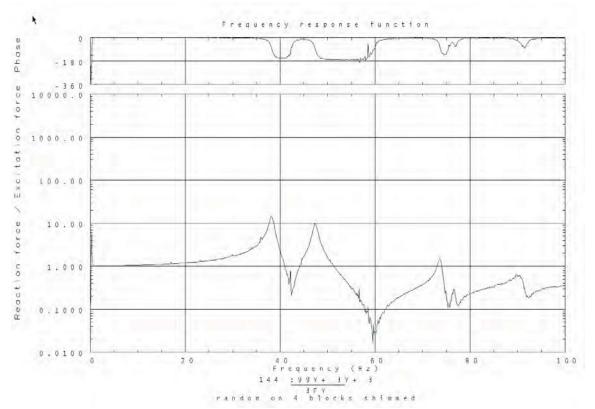| Dynamometer | | MATLAB | | Percent Error | |
|---|---|---|---|---|---|
| Static (lb-in) | Dynamic (lb-in$^2$) | Static (lb-in) | Dynamic (lb-in$^2$) | Static | Dynamic |
| 13.491 | 139.077 | 13.371 | 138.868 | 0.89% | 0.15% |
| (N-m) | (kg-m$^2$) | (N-m) | (kg-m$^2$) | | |
| 1.5243 | 0.040699 | 1.5107 | 0.040638 | | |



**Figure 6. Frequency Response Function of clamped dynamometer (without GMI)**
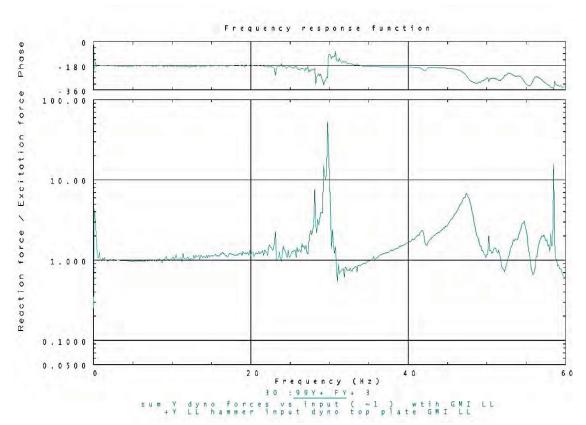
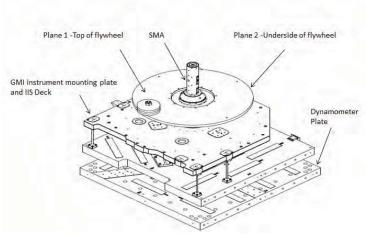Figure 7.  Frequency Response Function in configuration with GMI installed



Figure 8.  Spin Balance Risk Mitigation Test Setup

### Spin Balancing Verification of GMI

It is shown that GMI was adequately balanced to meet both static and dynamic balancing requirements. The measured imbalances in BRUTUS vacuum testing where found to be 0.017 kg-m (1.47 lbm-in) and 0.022 kg-m$^2$ (75.1 lb-in$^2$) meeting the requirements of 0.032 kg-m (2.78 lbm-in) static and 0.055 kg-m$^2$ (187 lb-in$^2$) dynamic imbalances, respectively. The results of Table 2 show the average of three separate measurements of forces, moments and computation of static and dynamic imbalances. Three tests are averaged to give imbalances in vacuum and three other tests carried in open air are averaged to determine final balancing values. All tests are run at 32 rpm and results show all tests met the

313

requirements. Other test runs, performed to acquire spin balance data at 28 rpm and 33 rpm, were also successful in showing that GMI successfully meets the balancing requirement.

The balancing of GMI takes place in two steps. In the first step, GMI is brought to a pseudo-balanced state, prior to assembling the RDA, MR, and final MLI layers in air in a cleanroom environment. In this configuration, analytical estimates of the RDA, MR, and MLI inertial properties are adopted while computing the balance masses, thus accounting for the future installation of these components. In the second step, the final balancing task is carried out while the fully assembled GMI in its final configuration in a vacuum chamber.

The MATLAB script reads the raw data file and pulls out the relevant ranges for the forces and resolver data. The resolver reading is first converted from the voltage pulse 'zero-crossing' point that, signals a full rotation, into useable angle data with respect to time. A correction value of 94.35 degrees (sensor location) is then added to the angular position to synchronize the zero position on the x–axis of the GICS coordinate system with the SMA resolver readings. This makes it possible to pinpoint the direction of the imbalance, as well as, to properly place balance masses in locations given in a single reference coordinate system. A total of nine forces are read as a function of time once every millisecond, one in each coordinate axis from each one of the three force transducers of the dynamometer. The data collected prior to the first resolver zero-crossing and after the last resolver zero-crossing time is disregarded. The force and moment resultants are then computed, and subjected to a low-pass Butterworth filter at 3 Hz. For each time station, the magnitude of the radial force and radial moment due to imbalance are computed, and plotted together with the static and dynamic imbalance magnitudes and directions as shown in Figure 9.

The mean radial force and mean radial moment are then computed and a linear programming solver is used to find the minimum set of masses that would simultaneously bring the static and dynamic imbalances back to a balanced state. The script has a set of 21 hard-coded mass locations with lower and upper bounds. The optimization is carried to satisfy the four constraint equations with an objective function equal to the sum of all masses as explained in the analytical section. As a default, each mass is equally favored. The user may elect to eliminate contributions from individual masses by bounding their individual lower and upper bounds to zero. Furthermore, the relevance of some weights can be affected through modifying their weights in the objective function. Once the optimization is carried successfully, the command window displays the statement "Optimization terminated." The solution is captured and displayed in three tables. The first table documents the magnitudes of the 21 masses, their locations and their first and second cross moment magnitudes. The resultant forces and moments due to the balancing masses are displayed in the second table. And finally the resultant static and dynamic inertial contributions from the balancing masses are shown in the third table. The initial properties of the imbalance are shown and compared to the solution. The magnitudes of the 21 balancing masses are also displayed in a bar graph for quick visualization. The balancing masses are displayed in their 3D locations as weighted, colored spheres together with the resultant mass. Also displayed are the resultant centrifugal force and moment produced by the balancing masses along with the imbalance radial force and moment. This gives a visual representation that a solution is found in which the balancing radial force and radial moment are equal in magnitude and directly opposite to the force and moment generated by the imbalances (see Figure 9).

The effect of the missing RDA/MR hardware on the static imbalance is based solely on its total mass and CG location. Because of this, it can be treated simply as the $22^{nd}$ balancing mass during the initial optimization process. This $22^{nd}$ presumed unknown mass will have the coordinates of the net CG of the missing RDA/MR assembly and its upper and lower mass bounds are set to the known total mass and inertial properties of the RDA/MR, so that when a solution is found, the $22^{nd}$ mass will be constrained to be equal to its known value.
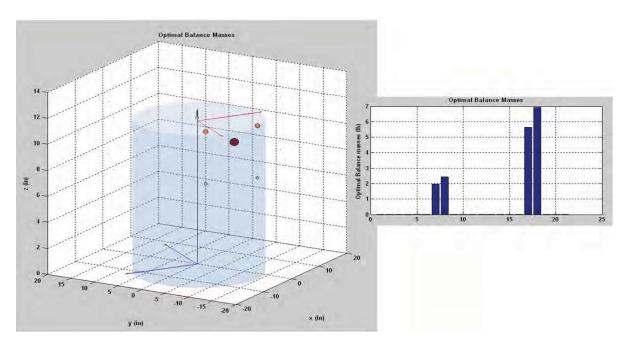
**Figure 9. Plot of Balancing masses, imbalance and balance force and bar graph**

Post Vibration Spin Balance Verification (without RDA/MR)
Following the completion of GMI vibration tests, the instrument was spun again on October 5, 2011 to compare with the pre-vibe imbalance measurements carried on August 2, 2011. The test is intended to check for possible shift of cabling and other flexible components. The difference between the two tests amounts to 0.26% in the radial force and 0.48% in the radial moment. It has to be noted that in addition to several changes to the stationary GMI hardware which theoretically would not affect the measurements (as long as we do not excite their modes), there have been slight changes in the configuration of rotating GMI that included the replacement of two 36 GHz flex wave guides, 0.0410 lb (0.183 N) each, with two rigid wave guides, 0.0168 lb (0.0747 N) each, and the re-machining of mounting shims. The wave guides along with the 36-GHz filter were re-staked, and one balance mass was removed, adjusted to account for the change, and then reinstalled in the same spot and re-staked. The overall delta is Wt = -0.051 lb (0.227 N). The new radial load is analytically evaluated and compared well with the measured value, placing all shifts at 0.106%, that is a delta of 0.005 lb (0.022 N), significantly less than the derived requirement of 0.08 lb (0.36 N) (or just 6.7% of the requirement). Therefore, it is safe to state that *vibration loads due to launch will likely shift the rotating mass by 7%, or less, of the requirement of 0.08 lb (0.36 N), on-orbit*.

In-Vacuum Final GMI Balancing
Several tests were carried out in vacuum and in air on the dynamometer to show that the requirements were met. It is worth noting that an RDA/MR deployment GSE off-loader structure needed to be removed from Brutus to perform clean test measurements. Table 2 shows the average of three separate measurements of forces, moments and computation of static and dynamic imbalances first in vacuum and then the averages of three other 32-rpm tests also run in the Brutus but in open air rather than in vacuum. Table 3 shows the computed and actual masses that brought GMI to meet requirements.

315

**Table 2. Average of imbalance measurements (three in vacuum and three in air)**

| units (lb,in) | Fx (lb) | Fy (lb) | Fr (lb) | Mx (lb·in) | My (lb·in) | Mr (lb·in) | me (lbm.in) | Jrz (lbm.in$^2$) |
|---|---|---|---|---|---|---|---|---|
| Vacuum | 0.0021 | 0.0402 | 0.0436 | -0.069 | 2.805 | 2.8 | 1.5 | 73.5 |
| Air | -0.0098 | 0.037 | 0.0398 | -0.86 | 1.104 | 1.5 | 1.4 | 63.9 |
| Requirement | | | 0.08 | | | 10 | 2.77 | 187 |

| units (Kg,m) | Fx (N) | Fy (N) | Fr (N) | Mx (N.m) | My (N.m) | Mr (N.m) | me (Kg.m) | Jrz (Kg.m$^2$) |
|---|---|---|---|---|---|---|---|---|
| Vacuum | 0.0092 | 0.1794 | 0.1946 | -0.008 | 0.318 | 0.318 | 0.017 | 0.022 |
| Air | -0.0438 | 0.1651 | 0.1775 | -0.097 | 0.125 | 0.167 | 0.016 | 0.019 |
| Requirement | | | 0.36 | | | 1.13 | 0.032 | 0.055 |



**Figure 10. GMI Integrated on the GPM Spacecraft at NASA Goddard Space Flight Center**

## Table 3. Added masses used to balance GMI

| Balance Mass Location ID | Desired (2) Brutus Spin Balance 2/4/12 (lbm) | Desired (2) Brutus Spin Balance 2/4/12 (kg) | Actual Brutues Spin Balance Final Values 2/9/12 (lbm) | Actual Brutues Spin Balance Final Values 2/9/12 (kg) |
|---|---|---|---|---|
| 1 | 0.198 | 0.090 | 0.196 | 0.089 |
| 2 | 5.25 | 2.38 | 5.25 | 2.38 |
| 3 | 1.495 | 0.6781 | 1.496 | 0.6786 |
| 4 | 0.19 | 0.086 | 0.19 | 0.086 |
| 5 | | | | |
| 6 | | | | |
| 7 | | | | |
| 8 | | | | |
| 9 | 10.17 | 4.613 | 10.17 | 4.613 |
| 10 | | | | |
| 11 | 0.063 | 0.029 | 0.064 | 0.029 |
| 12 | 0.393 | 0.178 | 0.394 | 0.179 |
| 13 | | | | |
| 14 | 2.77 | 1.26 | 2.77 | 1.26 |
| 15 | | | | |
| 16 | | | | |
| 17 | | | | |
| 18 | 0.006 | 0.003 | 0 | 0 |
| 19 | 0.34 | 0.15 | 0.34 | 0.15 |
| 20 | 0.205 | 0.0930 | 0.205 | 0.0930 |
| 21 | | | | |
| Total (lbm) | 21.08 | | 21.075 | |
| Total (kg) | | 9.562 | | 9.559 |

## Conclusion

The Global Microwave Imager instrument (GMI) was successfully spin-balanced using a dynamometer as a mounting fixture. GMI was balanced to less than 0.017 kg-m (1.47 lbm-in) static imbalance and 0.022 kg-m$^2$ (75.2 lb-in$^2$) dynamic imbalances, meeting the requirements of 0.032 kg-m (2.77 lbm-in) and 0.055 kg-m$^2$ (188 lb-in$^2$) respectively, total for the 123-kg (271-lb) spinning portion of the instrument payload.

The successful final precision spin balancing of the GMI instrument in vacuum demonstrated the capability of this method to accurately measure the static and dynamic imbalances, and to precisely compute the optimal set of minimal balance masses, accounting for various. The ability to precisely measure the imbalances before and after environmental testing also enabled us to very accurately predict the magnitude of the change in the GMI instrument imbalance on orbit, following launch.

The forces measured by the dynamometer checked well against two other independent measurement systems. In addition, the dynamometer is shown to be capable of reproducing the applied loads and moments with adequate accuracy. The natural structural frequencies of the dynamometer were mapped and their effect on the measurements was identified for the frequency spectrum of interest.

Prior to balancing GMI, both moderate and extreme imbalance risk mitigation tests are shown to be accurately measured using the dynamometer and the necessary balancing forces are accurately computed. The fully balanced state was also recovered from the time traces of the resultant radial loads and radial moments.

Since the successful completion of the final spin balance activity, the GMI instrument was delivered to Goddard Space Flight Center in March 2012, and was successfully integrated onto the GPM spacecraft later in June 2012, see Figure 10. The GPM spacecraft just recently completed spacecraft level Thermal

Vacuum (TVAC) testing in January 2013, vibration testing in July 2013, post-environmental testing in September 2013, and is scheduled to be launched in February 2014 from Tanegashima, Japan on a JAXA MHI-H11A rocket.

## References

1. Newell, D., Rait, G., Ta, T., Berdanier, B., Draper, D., Kubitschek, M., Krimchansky, S. "GPM Microwave Imager Design, Predicted Performance and Status", Proceedings of the 2010 IEEE International Geoscience and Remote Sensing Symposium (IGARSS) Publication Date: July 25, 2010.

2. Woolaway, S. Kubitschek, M., Berdanier, B., Newell, D., Dayton, C. and Pellicciotti, J. "GMI Spin Mechanism Assembly Design, Development, and Test Results", *Proceedings of 41th NASA Aerospace Mechanisms Symposium*, Langley Research Center, May 2012.

3. Koss, S., Woolaway, S. "Lessons Learned From the WindSat BAPTA Design and On-Orbit Anomalies", Proceedings of 38th NASA Aerospace Mechanisms Symposium, Langley Research Center, May 2006.

4. Pierre, W. "GMI Spin Mechanism Structural Analysis", BATC Internal SER Report No. 2307821B, Ball Aerospace and Technologies Corp., Nov. 2008.

5. Richard P. Wolley, Dynamic Balancing Without Spinning: A New Method for Unwieldy Satellites, SAWE paper No. 1670, Category 6.0, 44th Conference of the Society of Allied Weight Engineers, 1985.

6. Ayari, L. "Hybrid Testing & Simulation - The Next Step in Verification of Mechanical Requirements in the Aerospace Industry," Hybrid Simulation Theory, Implementation and Applications, Victor Saouma, Mettupalayam Sivaselva Editors, 2008.